Proceedings, 4th Chaotic Modeling and Simulation International Conference
31 May – 3 June 2011, Agios Nikolaos, Crete Greece

Falling of a Passive Compass-Gait Biped Robot Caused by a Boundary Crisis

Hassène Gritli[1], Nahla Khraief[2] and Safya Belghith[3]

National School of Engineers of Tunis, University of Tunis El Manar,
BP. 37, Le Belvédère, 1002 Tunis, Tunisia
E-mail:[1]grhass@yahoo.fr,
[2]nahla-khraief@yahoo.fr,
[3]safya.belghith@enit.rnu.tn

Abstract. The planar passive compass-gait biped robot on sloped surfaces is the simplest model of legged walkers. It is a two-degrees-of-freedom impulsive mechanical system known to exhibit, in response to an increase in the slope angle of the walking surface, a sequence of period-doubling bifurcations leading to chaos before falling down at some critical slope without any explanation. The fall is found to be occured with the abrupt destruction of chaos. We showed recently that a cyclic-fold bifurcation is also generated in the passive walking patterns of the compass robot. The aim of this paper is to show that the fall of the passive compass-gait biped robot occurs via a global bifurcation known as boundary crisis. We show that the cyclic-fold bifurcation is the key of the occurrence of such boundary crisis. We demonstrate how the same period-three unstable periodic orbit generated from the cyclic-fold bifurcation causes the abrupt death of chaos in the passive dynamic walking and hence the fall of the compass-gait biped robot.

Keywords: Compass-gait biped robot, Passive dynamic walking, Chaos, Cyclic–fold bifurcation, Boundary crisis..

1 Introduction

In the last decades, the robotic community has shown increasing interest in the field of biped robots. A key idea for natural and efficient walking of a biped robot is utilizing the dynamical property of the passive dynamic walking. This is a walking method which was first studied by McGeer in 1990 by exploring the behavior of the simplest passive biped robot known as the point-foot walker [1]. He showed in numerical simulations and experiments that such biped walking robot without controllers and actuators can walk steadily, stably and hence passively down some shallow inclined surfaces.

In addition, it is shown in several studies on passive-dynamic biped robots that the passive walk exhibits only a period-doubling route to chaos with respect to an increase in the slope angle of the ground. Such behavior transient is demonstrated with the point-foot walker [2], [9], the compass-gait model [3], [6], [8], the kneed models [4], and the torso-driven biped models [5], [13]. In this work, we deal with the compass-gait biped robot. Recently, we showed that the compass-gait biped exhibits also a cyclic-fold bifurcation where two period-three limit cycles (one stable and another unstable) meet and annihilate each other [7]. Moreover, the period-three stable limit cycle exhibits its own scenario of period-doubling bifurcations leading to the formation of chaotic gaits. In all these studies, the conventional period-doubling route to chaos will cause the sudden fall of the biped robot without any explanation. The only argument stressed is that the bipedal walk becomes completely chaotic which coincides with high speed of progression as well as with important step length of the compass-gait biped robot.

Walk models of biped robots are characterized by an impulsive nonlinear hybrid dynamics. A strong motivation to study such dynamics is the rich variety of surprising phenomena and the extremely complex behavior that possesses no counterpart in other nonlinear and linear systems. Examples are strange attractors, bifurcation routes to chaos and fractals structures. In this work, we focus on crisis [10] as a global bifurcation route to chaos in passive dynamic walking of the compass-gait biped robot. In the context of dynamical systems theory, a crisis is a global bifurcation provoking an abrupt change in a chaotic attractor as some control parameter of the system is varied [10]. In nonlinear dissipative systems, the most dramatic type of sudden change in chaotic attractor is a boundary crisis, in which a chaotic attractor abruptly disappears from the phase portrait [11]. Other important changes in chaotic attractor include interior crisis in which a strange attractor undergoes a sudden increase or decrease in size [12]. Both types of crisis involve in fact the tangency (or collision) of a chaotic attractor with an unstable periodic orbit. For the interior crisis, the tangency takes place in the interior of the basin of attraction of the chaotic attractor, whereas for the boundary crisis the tangency takes places on the boundary of the basin of attraction of the chaotic attractor. It is known so far that chaos and the boundary crisis appears in many complex nonlinear systems [14]-[20] . However, chaos, bifurcation and crisis have not been fully investigated in dynamic walking of biped robots. Recenlty, we revealed the presence of an interior crisis as route to chaos in the passive dynamic walking of the compass-gait biped robot and the torso-driven biped robot [21].

This work focuses only on the boundary crisis in the passive dynamic walking of the compass-gait biped robot. The aim of this study is to show that the onset/destruction of bipedal chaos can occur via the boundary crisis. We will demonstrate how the period-three unstable limit cycle born at the cyclic-fold bifurcation generates a double boundary crisis as a bifurcation parameter (slope angle) varies. We will show how such boundary crisis provokes the sudden death of a chaotic attractor and its basin of attraction causing hence the abrupt fall of the passive biped robot while walking down a sloped surface.

This paper is organized as follows: the compass-gait biped robot and its passive hybrid dynamics are presented in Section 2. Section 3 reveals the boundary crisis exhibited in the passive dynamic walking causing the fall of the compass-gait biped robot. Conclusion and future works are given in the last Section 4.

2 Passive hybrid dynamic of the compass-gait biped robot

2.1 The compass-gait biped robot

In order to investigate boundary crisis in passive dynamic walking, we utilize the compass-gait biped robot [3], [21] shown in Figure 1 descending a slope of angle φ. The compass robot is a passive two-degrees-of-freedom biped has a frictionless hip joint connecting two straight identical legs: a stance leg and a swing leg. The two legs are modeled as rigid bars. The hip has a mass m_H and each leg has a lumped mass m located at a distance b from the hip. While walking, the compass-gait biped robot is powered only by gravity without any actuation, and with an initial push it walks passively and indefinitely down the walking surface.

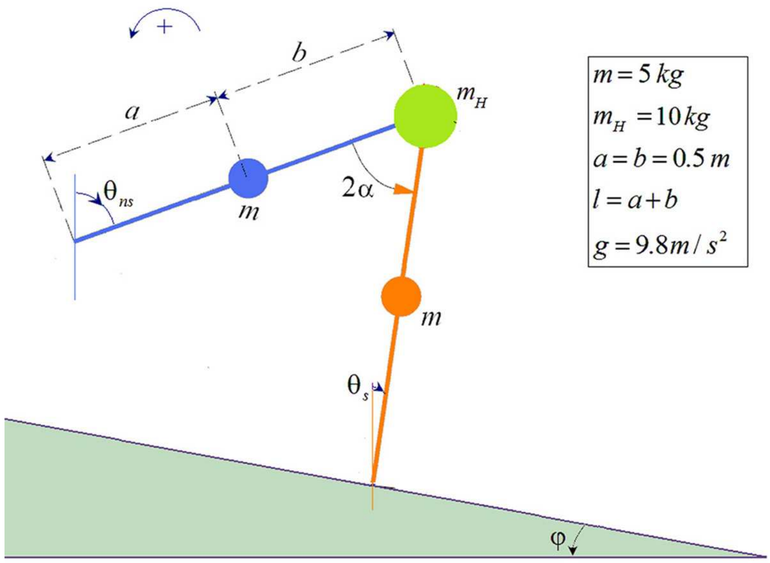

Fig. 1. A passive compass-gait biped robot down a sloped ramp of angle φ. On the right, physical parameters of the biped are listed.

The passive dynamic walking of the compass-gait biped robot as it goes down a sloped surface is constrained in the sagittal plane. It is made up primarily of two phases: a swing phase and a very instantaneous impact phase. The swing phase describes that one leg is fixed on the ground as a pivot and the other leg swings above the ground while walking down the slope of angle φ. The impact phase describes the instant when the swing leg strikes the ground after passing the stance leg. We make the standard assumptions that the impact is perfectly inelastic and that there is no slipping at the foot/ground contact. The bipedal walk configuration is determined by the support (stance) angle θ_s and the nonsupport (swing) angle θ_{ns}. The positive angles are computed counterclockwise with respect to the indicated vertical lines.

2.2 Hybrid dynamics of the compass-gait biped robot

The model of the passive dynamic walking of the compass-gait biped robot consists of nonlinear differential equations for the swing stage and algebraic equations for the impact stage [3]. Let $\theta = \begin{bmatrix}\theta_{ns} & \theta_s\end{bmatrix}^T$ be the vector of generalized coordinates. Under some standard assumptions noted before, the motion of the compass-gait biped robot can be described by the following hybrid nonlinear dynamics:

$$\mathcal{J}(\theta)\ddot{\theta} + \mathcal{H}(\theta,\dot{\theta}) + \mathcal{G}(\theta) = 0 \qquad if \quad \theta \notin \Gamma\,, \tag{1}$$

$$\theta^+ = \mathcal{R}\theta^- \quad and \quad \dot{\theta}^+ = \mathcal{S}\dot{\theta}^- \quad if \quad \theta \in \Gamma\,. \tag{2}$$

The first equation represents the swing phase, whereas the second one translates the impulsive impact stage. In (2), subscribes $^+$ and $^-$ denote just after and just before the impact phase, respectively. Given the slope angle φ of the walking surface, the impact surface Γ in (1) and (2) is defined by:

$$\Gamma = \left\{\theta \in \Re^2 \;:\; h(\theta) = \theta_{ns} + \theta_s + 2\varphi = 0\right\}, \tag{3}$$

Matrices in (1) and (2) are given by:

$\mathcal{J}(\theta) = \begin{bmatrix} mb^2 & -mlbcos(\theta_s - \theta_{ns}) \\ -mlbcos(\theta_s - \theta_{ns}) & m_H l^2 + m(l^2 + a^2) \end{bmatrix}$,

$\mathcal{H}(\theta,\dot{\theta}) = \begin{bmatrix} mlb\dot{\theta}_s^2 sin(\theta_s - \theta_{ns}) \\ -mlb\dot{\theta}_{ns}^2 sin(\theta_s - \theta_{ns}) \end{bmatrix}$, $\mathcal{G}(\theta) = g\begin{bmatrix} mbsin(\theta_{ns}) \\ -(m_H l + m(a+l))sin(\theta_s) \end{bmatrix}$,

$\mathcal{R} = \begin{bmatrix} 0 & 1 \\ 1 & 0 \end{bmatrix}$, $\mathcal{S} = \left(Q^+(\alpha)\right)^{-1} Q^-(\alpha)$,

$Q^-(\alpha) = \begin{bmatrix} -mab & -mab + (m_H l^2 + 2mal)cos(2\alpha) \\ 0 & -mab \end{bmatrix}$,

$Q^+(\alpha) = \begin{bmatrix} mb(b - lcos(2\alpha)) & ml(l - bcos(2\alpha)) + ma^2 + m_H l^2 \\ mb^2 & -mblcos(2\alpha) \end{bmatrix}$, and α is the half-interleg angle expressed by $\alpha = \frac{1}{2}(\theta_s - \theta_{ns})$.

3 Boundary crisis in the passive compass-gait model

It is well-known so far that the passive dynamic walking of the compass-gait biped robot exhibits only a period-doubling scenario route to chaos as the

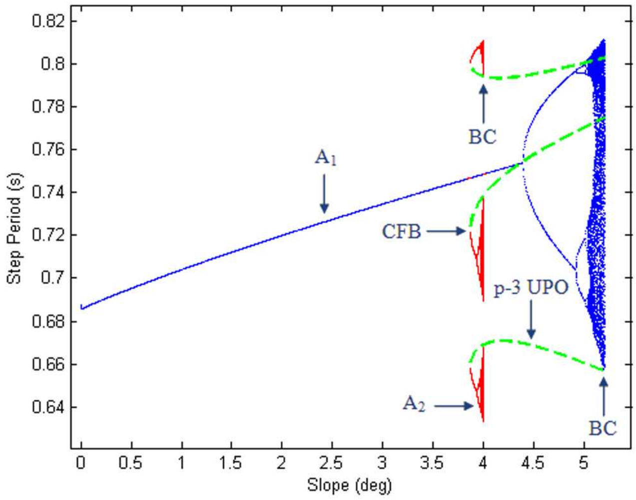

Fig. 2. Bifurcation diagram: step period as a function of slope angle φ.

slope angle φ increases [3]. The bifurcation diagram given by Figure 2 reveals such route to chaos (blue attractor A_1). The conventional attractor is observed for slopes between 0deg and 5.201deg. At this largest slope angle, the attractor A_1 is terminated and the compass-gait biped robot is found to fall down for higher slopes and only unstable gaits exists. However, this fall at such slope is not understood yet and the only reason given until nowadays is that the compass robot walks chaotically with high speeds and long steps which leads to its fall at some given slope which is here found to be 5.201deg. Figure 3 shows the conventional chaotic attractor A_1 for the slope angle $\varphi = 5.201$deg. Accordingly, for slopes higher than this critical value, the chaotic attractor does not exist and the biped robot falls down. Recently, we revealed the coexistence of another attractor with the conventional one in the compass-gait model [7]. Figure 2 shows this new attractor A_2 which is born via a cyclic-fold bifurcation (marked by CFB in Figure 2) at which two period-three gaits, one stable and another unstable, meet and annihilate each other. The cyclic-fold bifurcation is created at the slope $\varphi = 3.8734$deg. Obviously, the attractor A_2 is developed here to coexist with the period-one attractor A_1. Furthermore, it is clear that the period-three stable gait generates its own scenario of period-doubling route to chaos. Thus, at the slope angle $\varphi = 4.0035$deg, the chaotic attractor A_2 is suddenly disappeared and the gait switches to the period-one stable gait. Figure 4 plots the new chaotic attractor A_2 for the slope angle $\varphi = 4.0035$deg. Accordingly, in the passive walking patterns of the compass-gait biped robot, two co-existing period-doubling cascades route to chaos are observed. As mentioned before, the resulting period-three stable gait of the attractor A_2 undergoes a cascade of period-doubling bifurcations which lead to the formation of chaotic

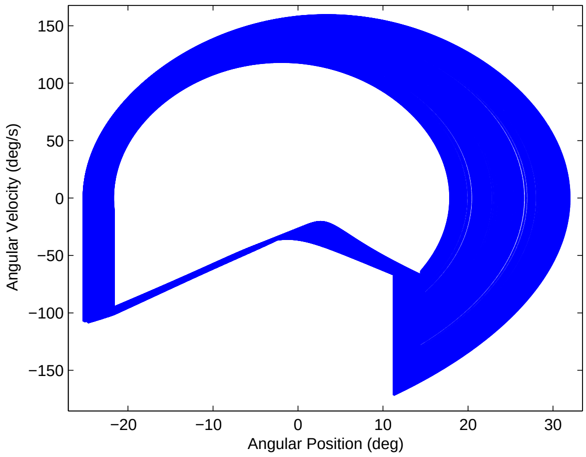

Fig. 3. Chaotic attractor of passive dynamic walking of the compass-gait biped robot down a slope of angle $\varphi = 5.201$deg.

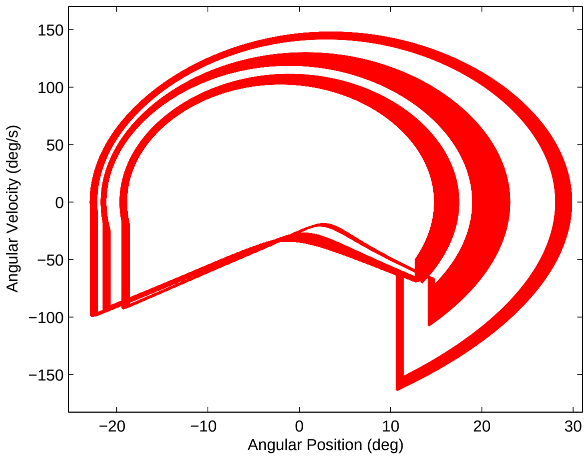

Fig. 4. Chaotic attractor of passive dynamic walking of the compass-gait biped robot down a slope of angle $\varphi = 4.0035$deg.

behaviors. The chaotic attractor A_2 of Figure 4 is destroyed abruptly at $\varphi_{BC} = 4.0035$deg with the unstable period-three orbit (p-3 UPO) created by the cyclic-fold bifurcation. Such event is known as boundary crisis (marked by BC in Figure 2). Indeed, a deep examination of Figure 2 shows that the occurrence of the boundary crisis is due to the collision of the chaotic attractor A_2 at its boundary with the period-three unstable periodic orbit. We emphasize that before the boundary crisis, two attractors A_1 and A_2 coexists, each with its own basin of attraction. However, the boundary crisis is found to kill the chaotic attractor A_2 and hence its basin of attraction. Accordingly, only the conventional attractor A_1 is survived after this boundary crisis.

In addition, it is evident that the p-3 UPO survives the first boundary crisis that causes the destruction of A_2 and continues to participate in the secondary boundary crisis that causes the abrupt destruction of the chaotic attractor A_1 at $\varphi_{BC} = 5.201$deg given by Figure 3. Hence, such double boundary crisis is generated in order to terminate the chaotic attractor A_1 and then to cause the fall of the compass-gait biped robot. We stress that the sudden disappearance/appearance of both chaotic attractors at the two crisis points involve the same p-3 UPO. Such event is called as a double boundary crisis [11]. We inform that the p-3 UPO is robust and persists after the destruction of chaotic attractor A1 where only unstable gaits exist.

4 Conclusion and future works

In this work, we have reported the main cause of the fall of compass-gait biped robot as it goes down an inclined slope. We have demonstrated that a global bifurcation known as the boundary crisis is occurred in the passive dynamic walking causing as consequence the fall. We have shown that a period-three unstable periodic orbit generated by a cyclic-fold bifurcation is the key for the characterization of the boundary crisis. We have analyzed in detail the role played by such unstable periodic orbit in the generation of a double boundary crisis which takes place to terminate the chaotic attractors and hence to be the main cause of the fall of the compass-gait biped robot.

In practice, the boundary crisis with its associated sudden death of a chaotic attractor is qualified as a dangerous event that can occur in nonlinear dynamics. Accordingly, it is worth mentioning that it will be very interesting to control such event of boundary crisis in the passive dynamic walking of the compass-gait biped robot in order to avoid the sudden death of an attractor and its basin of attraction. The numerical tools developed in this paper can be applied to the detection of boundary crisis and other nonlinear phenomena in some other biped robots.

References

1.T. McGeer. Passive dynamic walking. *The International Journal of Robotics Research*, 9(2): 62-68, 1990.
2.M. Garcia, A. Chatterjee, and A. Ruina. Efficiency, Speed, and Scaling of Two-Dimensional Passive-Dynamic Walking. *Dynamics and Stability of Systems*, 15(2):75-99, 2000.
3.A. Goswami, B. Thuilot, and B. Espiau. A study of the passive gait of a compass-like biped robot: symmetry and chaos. *International Journal of Robotics Research*, 17(12):1282-1301, 1998.

4.P. Zhang, Y. Tian, Z. Liu, S. Yang, and R. Tian. Further research and comparison of gaits for compass-like biped and kneed passive dynamic walker. *International Conference on Intelligent Robotics and Applications*, 1216-1226, 2008.
5.T. Narukawa, M. Takahashi, and K. Yoshida. Biped Locomotion on Level Ground by Torso and Swing-Leg Control Based on Passive-Dynamic Walking. *IEEE/RSJ International Conference on Intelligent Robots and Systems*, 4009-4014, 2005.
6.J. S. Moon, and M. W. Spong. Bifurcations and chaos in passive walking of a compass-gait biped with asymmetries. *International Conference on Robotics and Automation*, 1721-1726, 2010.
7.H. Gritli, N. Khraeif, and S. Belghith. Cyclic fold bifurcation route to chaos in passive bipedal walking. *International Conference on Informatics in Control, Automation and Robotics*, 2010, accepted.
8.H. Gritli, N. Khraeif, and S. Belghith. Cyclic-Fold Bifurcation in Passive Bipedal Walking of a Compass-Gait Biped Robot with Leg Length Discrepancy. *IEEE International Conference on Mechatronics*, 2011.
9.A. T. Safa, M. G. Saadat, and M. Naraghi. Passive dynamic of the simplest walking model: Replacing ramps with stairs. *Mechanism and Machine Theory*, 42, 1314-1325, 2007.
10.C. Grebogi, E. Ott, and J. A. Yorke. Crises: Sudden Changes in Chaotic Attractors and Chaotic Transients. *Physica D*, 7, 181-200, 1983.
11.A. C.-L. Chian, F. A. Borotto, and E. L. Rempel. Alfven boundary Crisis. *International Journal of Bifurcation and Chaos*, 12(7): 1653-1658, 2002.
12.F. A. Borotto, A. C.-L. Chian, and E. L. Rempel. Alfven Interior Crisis. *International Journal of Bifurcation and Chaos*, 14(7): 2375-2380, 2004.
13.H. Gritli, N. Khraeif, and S. Belghith. Semi-Passive Control of a Torso-Driven Compass-Gait Biped Robot: Bifurcation and Chaos. *IEEE International Multi-Conference on Systems, Signals and Devices*, 2011.
14.L. Hong, Y. Zhang, and J. Jiang. A Boundary Crisis in High Dimensional Chaotic Systems. *Dynamical Systems: Discontinuity, Stochasticity and Time-Delay*, Part 1, 31-36, 2010.
15.H. M. Osinga, and U. Feudel. Boundary crisis in quasiperiodically forced systems. *Physica D*, 141, 54-64, 2000.
16.W. Z. Stupnicka, A. Zubrzycki, and E. Tyrkiel. Properties of Chaotic and Regular Boundary Crisis in Dissipative Driven Nonlinear Oscillators. *Nonlinear Dynamics*, 19, 19-36, 1999.
17.W. S. Stupnicka, and K. L. Janicki. Basin boundary bifurcations and boundary crisis in the twin-well Duffing oscillator: Scenarios related to the saddle of the large resonant orbit. *International Journal of Bifurcation and Chaos*, 7(1):129-146, 1997.
18.H. B. Stewart, Y. Ueda, C. Grebogi, and J. A. Yorke. Double crises in two-parameter dynamical systems. *Phys. Rev. Lett.*, 75(13):2478-2481, 1995.
19.J. M. T. Thompson, H. B. Stewart, and Y. Ueda. Safe, explosive and dangerous bifurcations in dissipative dynamical systems. *Physical Review E*, 49(2):1019-1027, 1994.
20.J. A. C. Gallas, C. Grebogi, J. A. Yorke. Vertices in parameter space: double crises which destroy chaotic attractors. *Phys. Rev. Lett.*, 71(9):1359-1362, 1993.
21.H. Gritli, S. Belghith, and N. Khraeif. Intermittency and Interior Crisis as Route to chaos in Dynamic Walking of two Biped Robots. *International Journal of Bifurcation and Chaos*, 2011, submitted.

Proceedings, 4th Chaotic Modeling and Simulation International Conference
31 May – 3 June 2011, Agios Nikolaos, Crete Greece

Flux Optimization in Field Oriented Control for Induction Machine Drives

Said GROUNI, Madjid KIDOUCHE

M'Hamed Bougara University of Boumerdes, Faculty of sciences, Physics Department, Boumerdes, 35000, Algeria
E-mail: said.grouni@yahoo.com , kidouche_m@hotmail.com

Abstract: This paper presents a novel strategy to control an induction machine drives with optimum rotor flux that minimizes the power loss under practical currents, voltages and position measurements. Based on strategy of flux optimization method, the implementation of indirect field oriented control for induction machine drives is realised. The improved practical control models are evaluated and confirmed through experiments using an induction machine (1.5kW/380V). Simulations tests are provided to evaluate the performance of the control scheme system.
Keywords: Optimization, Flux, Field Oriented Control, Induction Machine.

1. Introduction

Induction motors are, without any doubt, the most used in more industrial applications, G.K. Singh, 2005 [1]. Nowadays, loss optimization with optimum flux control is a topic in electrical drives for both scalar controlled and vector controlled induction motor drives. Different approaches have been recently proposed in the literature A.C. Machado and all, 2008 [2], R. Marino and all, 2008 [3], J.Q. Ren and all, 2008 [4], C. Thanga Raj and all, 2009 [5], S. Abourida and all, 2009 [6]. Adaptive control, fuzzy logic and neural networks and real time power loss with loss minimization techniques are new being increasingly applied to optimization control variable frequency drives, S. Abourida and all, 2009 [6], A.M. Bazzi and all, 2009 [7]. The philosophy of optimization flux control is based on using optimum flux condition that minimizes losses with respect to air gap flux at steady state operation G.K. Singh, 2005 [1], A.M. Bazzi and all, 2009 [7], S.C. Englebreston and all, 2008 [11], R. Leidhold and all, 2002 [12]. However, to keep the drive performance, some physical limitations must be taken into account, S. Grouni and all, 2008 [9], G. W. Chang and all, 2001 [10], B. Wang and all, 2007 [17], A.S. Bezanella and all, 2001 [18].

The first restriction is concerned with the stator current amplitude. As the induction motor flux is decreased, depending on the load torque condition. The stator current may be bigger than its rated value, what cause the destruction of the drive by over current.

The second limitation is that the flux must not be decreased null. At each load torque, there exists a necessary minimum flux to keep the speed at the reference command value. In field oriented vector control induction motor drive this minimum flux does not only depend on the flux current ids, but also on the torque current i_{qs} as it will be shown later.

Other important aspect is the loss of electromagnetic torque in the induction motor. As the flux is decremented, the torque capability is reduced, F.F. Bernal and all, 2000 [19].

In this paper, these restrictions are studies analytically for an indirect vector controlled induction motor drives. Finally, different models of control are proposed at steady state to avoid the control problem of the drive.

This paper presents the problem formulation of control optimum rotor flux that optimizes total energy under practical measurements variables of currents, voltages and position. Based on the mathematical dynamic model that used the induction motor model, physics-based methods that search for the minimum power loss regardless of the motor model or parameters. The practical application of our control models are evaluated and confirmed through experiments using an induction motor (1.5kW/380V). Simulations and experimental investigation tests are provided to evaluate the consistency and performance of the proposed control model.

2. Mathematical model of control flux formulation

The mathematical model of vector controlled induction motor drive is available in literature J. Holtz and all, 2002 [13], J. Holtz and all, 2006 [14], R. Krishnan, 2001 [16]. The mathematical function of motor flux and load torque is considered in (d, q) reference frame with synchronously rotating speed with stator current [15], R. Krishnan, 2001 [16], P. Vas, 1990 [21].

In this analysis of mathematical model, we are assuming of parasitic effects such as hysteresis, eddy currents and magnetic saturation are neglected. And an ideal behaviour of inverter, what implies the actual motor currents are equal to the reference commands therefore, the load torque at steady state must be equal to the electromagnetic torque developed by the machine. The function of d,q stator currents is defined:

$$|I_s| = \sqrt{(i_{ds})^2 + (i_{qs})^2} \tag{2.1}$$

where i_{ds} is the direct current or flux current component, and i_{qs} is the quadrate current or torque current component and I_s is the current circulation by the stator windings. Moreover, the electromagnetic torque C_{em} which is the same as the load torque at steady state condition can be expressed by:

$$C_{em} = k_t (i_{ds} i_{qs}) \tag{2.2}$$

where k_t is a positive number.

Manipulating both equations (2.1) and (2.2), yields the stator current amplitude as a function of load torque and flux current component:

$$\left|I_s\right| = \sqrt{\left(\frac{C_{em}}{k_t i_{ds}}\right)^2 + \left(i_{ds}\right)^2} \tag{2.3}$$

If the load torque is assumed to be constant at steady state, the minimum of the stator current function (2.3) is achieved when:

$$\frac{d\left|I_s\right|}{di_{ds}} = \frac{i_{ds} - \dfrac{\left(C_{em}\right)^2}{k_t^2 \left(i_{ds}\right)^3}}{\sqrt{\left(\dfrac{C_{em}}{k_t i_{ds}^*}\right)^2 + \left(i_{ds}\right)^2}} \tag{2.4}$$

which yields the relative minimum condition when the stator flux current is:

$$i_{ds}\Big|_{\left|I_s\right|_{\min}} = \sqrt{\frac{C_{em}}{k_t}} \tag{2.5}$$

This minimum existence condition when (2.4) is equal at zero requires the second derivative of equation (2.3) will be positive for every torque which k_t is constant number.

However, if the flux current is too small, the stator current amplitude may become bigger than its rate value. It can be observed that at each flux current, the stator current is a function depending on the torque. At light loads, the stator current with reduced flux is smaller than the corresponding with the rated flux. In this case, special care must be taken in order to avoid the destruction of the drive, as well as the motor, by over current.

3. Minimum flux function of control problem

At steady state condition, the allowed maximum current must be the rated current to avoid the destruction of the drive as well as the motor. The expression of stator current is given by:

$$\left|I_s\right| \le \sqrt{2}\left|I_s\right|_{RMS}^{rated} \tag{3.1}$$

As before, developed and manipulating equation (2.1), (2.2) and (2.3) which yields a biquadratic equation, whose positive solutions are:

$$i_{ds} = \sqrt{\frac{I_s^2 \pm \sqrt{I_s^4 - 4\left(\dfrac{C_{em}}{k_t}\right)^2}}{2}} \tag{3.2}$$

Therefore, the expression for the necessary minimum flux current at each load torque is:

$$i_{ds} = \sqrt{\frac{I_s^2 - \sqrt{I_s^4 - 4\left(\dfrac{C_{em}}{k_t}\right)^2}}{2}} \tag{3.3}$$

It means the lowest value of the stator flux current needed to develop the torque required by the load.

Finally, the flux current reference must always be:

$$i_{ds} \le \sqrt{I_s^2 - {i_{qs}}^2} \tag{3.4}$$

at every torque in order to keep the drive performance.

4. Model loss of electromagnetic torque control

The maximum current circulating by stator winding is given by:

$$\left|I_s\right| = \sqrt{{i_{ds}}^2 + {i_{qs}}^2} \le \left|I_s\right|_{\max} \tag{4.1}$$

If we consider the maximum stator current as its rated value, we get the expression:

$$\frac{C_{em}\Big|_{i_{ds}}}{C_{em}\Big|_{i_{ds}^{rated}}} = \frac{i_{ds}\sqrt{\left(I_s^{\max}\right)^2 - \left(i_{ds}\right)^2}}{i_{dsrated}\sqrt{\left(I_s^{\max}\right)^2 + \left(i_{dsrated}\right)^2}} \tag{4.2}$$

And

$$\frac{C_{em}\Big|_{i_{ds}}}{C_{em}\Big|_{i_{ds}^{rated}}} = \left(\frac{i_{ds}}{i_{dsrated}}\right)^2 \frac{\sqrt{\left(\frac{I_s^{\max}}{i_{ds}}\right)^2 - 1}}{\sqrt{\left(\frac{I_s^{\max}}{i_{dsrated}}\right)^2 + 1}} \tag{4.3}$$

This expression represents the loss of electromagnetic torque capability, as a function of flux current. In other words, this expression stands for the maximum available torque at each flux. At rated torque, the flux current cannot be smaller that its rated value, and in theory, at no load, the flux can be decreased to zero. In an actual drive, this would suppose the demagnetization of the machine, causing the motor stop.

5. Optimization power loss in vector controlled motor

The optimization power loss of an indirect vector controlled induction motor drives including the electrical and magnetically losses and mechanical losses are the most used in the literature A.C. Machado and all, 2008 [2], J.Q. Ren and all, 2008 [4], A.M. Bazzi and all, 2009 [7], S. Grouni and all, 2008 [9], F. Abrahamsen and all, 1997 [20], P. Vas, 1990 [21].
In order to calculate the power loss, the following model from is used:

$$P_e = v_{ds}i_{ds} + v_{qs}i_{qs} \tag{5.1}$$

The expression of electromagnetic total power is yield in dynamic regime:

$$\begin{aligned} P_e = {} & \sigma L_s\left(i_{ds}\frac{di_{ds}}{dt} + i_{qs}\frac{di_{qs}}{dt}\right) - \frac{1}{L_r}\left(\frac{d\varphi_{dr}}{dt}\varphi_{dr} + \frac{d\varphi_{qr}}{dt}\varphi_{qr}\right) \\ & + R_s\left(i_{ds}^2 + i_{qs}^2\right) - R_r\left(i_{dr}^2 + i_{qr}^2\right) + \frac{L_m}{L_r}\omega\left(\varphi_{dr}i_{qs} - \varphi_{qr}i_{ds}\right) \\ & - \frac{2R_rL_m}{L_r}\left(i_{qr}i_{qs} + i_{qs}i_{ds}\right) \end{aligned} \tag{5.2}$$

The total power loss is given by:

$$\Delta P_t = \left(R_s + \frac{R_rL_m^2}{L_r^2}\right)\left(i_{ds}^2 + i_{qs}^2\right) + \left(\frac{R_rL_m^2}{L_r^2} + R_f\right)\left(\frac{\varphi_r}{L_m}\right)^2 - \frac{R_rL_m}{L_r^2}i_{ds}\varphi_r \tag{5.3}$$

where (ω_s , ω) are the synchronous and mechanical rotor speeds of machine, (R_s , R_r) are resistances of stator and rotor, (i_{ds}, i_{qs}) and (i_{dr} , i_{qr}) are the d-q axis equivalent stator and rotor currents, (φ_{ds} , φ_{qs}) and (φ_{dr} , φ_{dr}) are the d-q axis flux linkages of the stator and rotor.

The solution of optimization problem can easily show that optimal flux depends only of differential flux function. Optimum operation point, corresponding to minimum loss is obtained by differentiating (14) upon the component of the rotor flux, where β is a positive number:

$$\frac{\partial P_t}{\partial \varphi_r} = 0 \tag{5.4}$$

$$\varphi_r^{opt} = \beta \sqrt{|C_{em}|} \tag{5.5}$$

$$\beta = \left(\frac{L_r^2 R_s + R_r L_m^2}{(R_s + R_f) p^2} \right)^{1/4} \tag{5.6}$$

The optimal control is then found to be:

$$u_1^o = \frac{T_r}{L_m} \left(\frac{d\varphi_r^{opt}}{dt} + \frac{1}{T_r} \varphi_r^{opt} \right) \tag{5.7}$$

The Fig.1 shows the block diagram of control drives. It consists of the following equipment:

- An industrial variable frequency drive (inverter-converter) of 1.5 kW that provides a three phase voltage with variable magnitude and frequency.
- A three phase squirrel cage induction motor, with the following nameplate data in appendix.

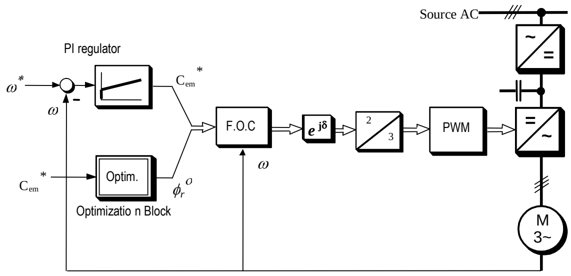

Fig.1. Scheme of block diagram control

To validate the proposed control scheme, the numerical results of stator current and losses are obtained as follows:

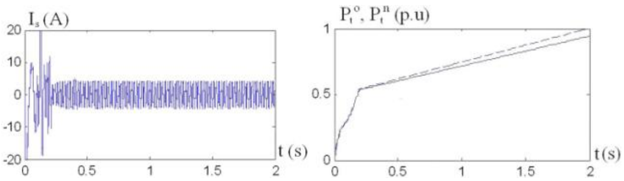

a) Stator current response **b) Power loss response**

Fig.2. Simulation results with control flux for optimization loss

In Fig.2, the behavior of the drive is shown under low load condition. It shows simulation results in indirect field oriented control of respectively the power loss at nominal and optimum fluxes operating in both transient and steady state. The graph shows successfully the waveform of stator current with imposing an optimum flux reference; we have obtained an improvement control loss optimization.

6. Optimization loss with current function $i_{ds} = f(i_{qs})$

The loss optimization is given by using the objective function linking two components of stator current for a copper loss minimization. The expression of power losses is given by:

$$\Delta P_t = \sigma L_s \left(i_{ds} \frac{di_{ds}}{dt} + i_{qs} \frac{di_{qs}}{dt} \right) - \frac{L_m}{T_r L_r} \varphi_{dr} i_{ds} + \left(R_s + \frac{L_m^2}{L_r T_r} \right) \left(i_{ds}^2 + i_{qs}^2 \right), \tag{6.1}$$

In steady state, the stator current expression at minimum power loss is:

$$i_{ds} = \left(1 + \frac{L_m^2}{R_s L_r T_r} \right)^{\frac{1}{2}} i_{qs} \tag{6.2}$$

In Fig.3, simulation results of stator current and power loss are presented. In order, to confirm the proposed control, we are taking into account of deviation motor parameters. The adaptation on line of rotor resistance is applied. The torque and speed responses in transient and steady state are obtained with rotor flux control. The responses of power loss have shown a reduced power loss.

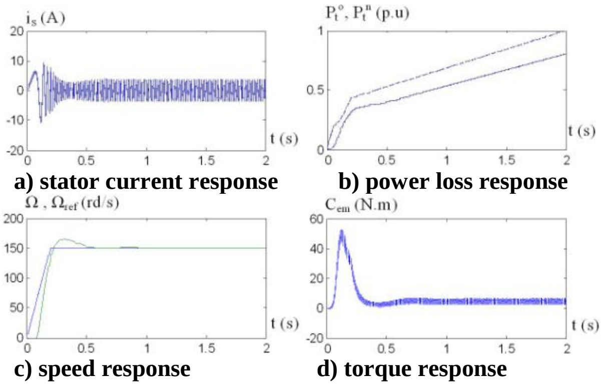

a) stator current response
b) power loss response
c) speed response
d) torque response

Fig.3. Simulation results with flux variation control

The comparison between loss minimization in Fig.2 and Fig.3 shows the improved response with iron and core losses parameters variations.

7. Optimization loss using the function $i_{ds} = f(i_{qs}, \omega)$

Loss optimization is presented by introducing the mechanical phenomena. Copper and iron losses are given:

$$\Delta P_v = R_s \left(i_{ds}^2 + i_{qs}^2 \right) + \frac{R_r R_f}{R_r + R_f} i_{qs}^2 - \frac{L_m^2 \omega^2}{R_r + R_f} i_{ds}^2 \tag{7.1}$$

The expression of stator current that gives the minimum loss at the steady state is given by:

$$i_{ds} = \sqrt{\frac{R_s R_r + R_s R_f + R_r R_f}{L_m^2 \omega^2 - R_s \left(R_r + R_f \right)}}\, i_{qs} \tag{7.2}$$

The improved control design for an optimal process rotor flux is given by the following scheme block diagram:

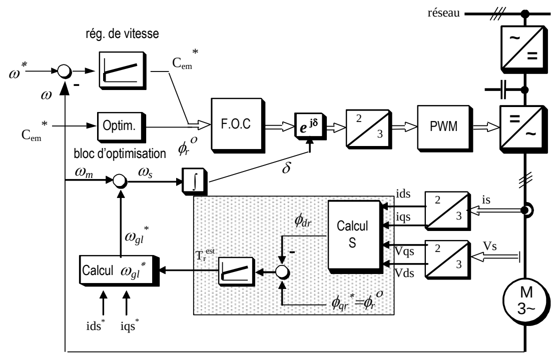

Fig. 4. Optimal control system for minimization loss

The control system proposed consists of two parts: one for keeping the speed at the reference value in steady state, combined with the continuous search for the point of minimum electric losses, and the other to create the optimal transient process. In this control, we are taking into account the motor current limitation restriction, which is the limit current fixed for the motor, not higher than the minimum between the maximum admissible currents of the inverter and the motor. In order, this optimal flux control is based on the variation value of the rotor electromagnetic time constant, which this constant is adapted in the control induction drives.

In Fig.4, we represent the simulation responses of stator current and power loss also the response of speed and torque. In order, the speed response follows perfectly the reference in steady state. The reduced losses are obtained by including the mechanical friction.

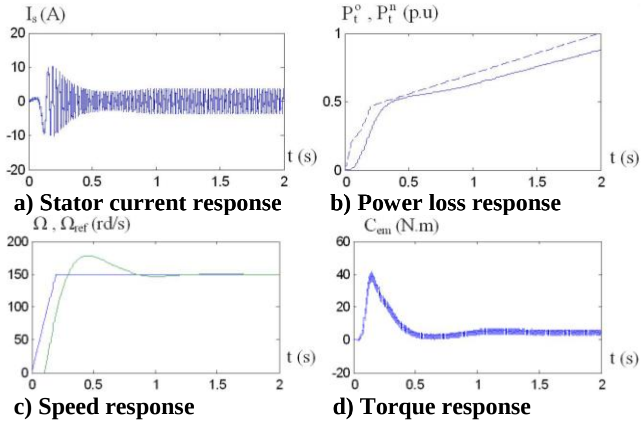

Fig. 4. Simulation responses including mechanical phenomena

8. Conclusion

In this paper, we have presented the loss optimization in indirect field oriented control with optimum flux for induction motor drives. We are taking account of parameters variation. We are obtained the optimum flux in real time. Simulation responses were presented. Finally, this control achieves a good performance of induction machine drives.

Appendix

induction motor parameters: P_n= 1.5 kW, U_n= 380/220 V, Ω_n= 1420 rpm, I_n= 3.64 A(Y) 6.31A(Δ), R_s= 4.85Ω, R_r= 3.805Ω, L_s= 0.274 H, L_r= 0.274 H, p= 2, L_m= 0.258 H, J= 0.031 kg.m^2, f_r= 0.008 Nm.s/rd.

References

1. G.K. Singh. A research survey of induction motor operation with non-sinusoidal supply wave forms, *Electric Power System Research* SCIENCE DIRECT ELSEVIER 75: 200-213, 2005.
2. A.C. Machado, E. Pacheco João, M.V. Ferreirada Luz, C.G.C. Neves, R. Carlson. Stray load losses calculation routine based on the Eh-star method, *Proceedings of the International Conference on Electrical Machines*, 1-4, 2008.
3. R. Marino, P. Tomei, C.M. Verrelli, An adaptive tracking control from current measurements for induction motors with uncertain load torque and rotor resistance, *Journal Automatica*, vol.44, no.11, 2593-2599, 2008.
4. J.Q. Ren, Y.H. Ii., W. Xu, K. Wang, Loss model establishment and efficiency optimization control of single sided linear induction motor, *IEEE Trans. Ind. Elec.* vol. 43, no.1, 226-231, 2008.
5. C. Thanga Raj, S.P. Srivastava, P. Agarwal. Particle swarm and fuzzy logic based optimal energy control of induction motor for a mine hoist load diagram, *IAENG international journal of computer science*, IJCS 36:1:03, 2009.
6. S. Abourida, J. Belanger, Real time platform for the control prototyping and simulation of power electronics and motor drive, *Proc. of the third International Conference on Modeling, Simulation and Applied Optimization (ICMSAO)*, Shariah, U.E.A., 20-22, 2009.
7. A.M. Bazzi, P.T. Krein. A survey of real time power loss minimizes for induction motors, *IEEE Trans. Ind. Elec*. vol. 43, no.1, 226-231, 2009.
8. Y. H. Chang, J.C. Chang, C.J Lee, Y.Y. Wang. Modeling and QFT based design of vector control induction motors, *Journal of the Chinese Institute of Engineers JCIE*, vol. 24, no.4, 473-485, 2001.
9. S. Grouni, R. Ibtiouen, M. Kidouche, O. Touhami. Improvement approach on rotor time constant adaptation with optimum flux in IFOC for induction motors drives, *Int. Journal of Mathematical, Physical and Eng. Sciences*, vol. 2, no. 3, 121-125, 2008.
10. G. W. Chang, J.P. Hespanha, A. S. Morse, M.S. Netto, R. Ortega. Supervisory field oriented control of induction motors with uncertain rotor resistance, *International Journal of Adaptive Control and Signal Processing*, vol.15, 353-375, 2001.
11. S.C. Englebreston, J.L. Kirtley. Induction motor stray losses and inter-bar currents, *Proceedings of the International Conference on Electrical Machines*, 1-5, 2008.
12. R. Leidhold, G. Garcia, M.I. Valla. Field oriented controlled induction generator with loss minimization, *IEEE Trans. on Ind*. Elec. vol.49, no.1, 147-155, 2002.
13. J. Holt. Sensorless control of Induction Machines- with or without Signal Injection? Overview Paper, *IEEE Trans. on Ind. Elect*. vol. 53, no.1,7-30, 2006.
14. J. Holtz, J. Quan. Sensorless control of induction motor drives, *Proceedings of IEEE*, vol. 90, no.8, 1359-1394, 2002.

15. P.C. Krause, O. Wasynczuk, S.D. Sudhoff, *Analysis of Electric Machinery*, McGraw Hill, USA, 1986.
16. R. Krishnan. *Electric Motor Drives, Modeling, Analysis and control*, Prentice Hall, 2001.
17. B. Wang, M. Chiasson & Bodson, L. M. Tolbert. An online rotor time constant estimator for the induction machine, *IEEE, Trans. Contr. Syst. Techno.*, vol. 15, no.2, 339-347, 2007.
18. A.S. Bezanella, R. Reginetto. Robust tuning of the speed loop in indirect field oriented control induction motors, *Journal Automatica*, vol. 03, 2001, pp. 1811-1818.
19. F.F. Bernal, A.G. Cerrada, R. Faure. Model based loss minimization for DC and AC vector controlled motors including core saturation, *IEEE Trans. on Ind. App.* vol.36, no.3, 755-763, 2000.
20. F. Abrahamsen, F. Blåbjer, J.K. Pederson. Analysis of stability in low cost energy optimal controlled PWM VSI fed induction motor drive. *Proceedings of EPE'97 Trondheim*, 3.717-3.723, Norway, 1997.
21. P. Vas. *Vector Control of AC Machines*, Oxford, Clarendon Press, 1990

Similarity Measure for Fuzzy Numbers

Tayebeh Hajjari

Islamic Azad University, Firuz-Kuh Branch, Firuz-Kuh, Iran
E-mail: tayebehajjari@iaufb.ac.ir

Abstract: Ranking of fuzzy numbers plays a very important role in linguistic decision-making and some other fuzzy application sys- terms. Several strategies have been proposed for ranking of fuzzy numbers. Each of these techniques has been shown to produce non-intuitive results in certain case. This paper proposes a new similarity measure to calculate the degree of similarity of generalized fuzzy numbers. The similarity measure is developed by integrating the concept of centre of gravity points and fuzzy difference of distance of points of fuzzy numbers. A fuzzy description for difference of distances between fuzzy numbers in its turn exploits appropriate similarity measure between the pattern sets when compared with other measures available. It greatly reduces the influence of inaccurate measures and provides a very intuitive quantification. Several sets of pattern recognition problems and a fingerprint-matching problem are taken to compare the proposed method with the existing similarity measures. Our approach gives a better and more robust similarity measure.
Keywords: Magnitude of fuzzy numbers, Parametric form of fuzzy numbers, Ranking, Trapezoial fuzzy numbers.

1. Introduction

Ranking of fuzzy numbers is an important component of the decision process in many applications. Many fuzzy ranking indices have been proposed since 1976. In 1976 and 1977, Jain [1,2] proposed a method using the concept of maximizing set to order the fuzzy numbers. Jain's method is that the decision maker considers only the right side membership function. A canonical way to extend the natural ordering of real numbers to fuzzy numbers was suggested by Bass and Kwakernaak [3] as early as 1977. Dubios and Prade 1978 [4], used maximizing sets to order fuzzy numbers. In 1979, Baldwin and Guild [5] indicated that these two methods have some disturbing disadvantages. Also, in 1980, Adamo [6] used the concept of α-level set in order to introduce α-preference rule. In 1981 Chang [7] introduced the concept of the preference function of an alternative. Yager in 1981 [8, 9] proposed four indices which may be employed for the purpose of ordering fuzzy quantities in [0, 1]. Bortolan and Degani have been compared and reviewed some of these ranking methods [10]. Chen and Hwang [11] thoroughly reviewed the existing approaches, and pointed out some illogical conditions that arise among them. Chen [12], Choobineh [13], Cheng [14] have presented some methods, and also more recently numerous ranking techniques have been proposed and investigated by Cha and Tsao [15] and Ma, Kandel and Friedman [16]. Nowadays many researchers have developed methods to compare and to rank fuzzy numbers. Some of those methods are counter-intuitive and non-discriminating [17, 18, 19, 20, 21] and recently some methods based on different distance functions have been

introduced for ranking of fuzzy numbers [22, 23, 24, 25, 26, 27]. In 2007 Asady and Zendehanm [28] employed distance minimization to rank fuzzy numbers. Then Abbasbandy and Hajjari [24] found a shortcoming on their method, therefore they presented a new method for ranking trapezoidal fuzzy numbers.
In 2010 Asady [29] revised the distance minimization method and introduced epsilon-neighborhood as a development of distance minimization. Now it is found that there is a drawback on their correction.
The rest of the paper is organized as follows. Section 2 contains the basic definitions and notations use in the remaining parts of the paper. Section 3 includes a new method to rank fuzzy numbers and a numerical example to compare the proposed method with the previous one. The paper is concluded in Section 4.

2. Back ground Information

2.1 Defiition

First, In general, a generalized fuzzy number A is membership $\mu_A(x)$ can be defined as [2]

$$\mu_A(x)=\begin{cases} L_A(x) & a\le x\le b \\ \omega & b\le x\le c \\ R_A(x) & c\le x\le d \\ 0 & otherwise, \end{cases} \tag{1}$$

Where $0\le\omega\le 1$ is a constant, and $L_A:[a,b]\to[0,\omega]$, $R_A:[c,d]\to[0,\omega]$ are two strictly monotonical and continuous mapping from R to closed interval $[0,\omega]$. If $\omega=1$, then A is a normal fuzzy number; otherwise, it is a trapezoidal fuzzy number and is usually denoted by $A=(a,b,c,d,\omega)$ or $A=(a,b,c,d)$ if $\omega=1$.
In particular, when $b=c$, the trapezoidal fuzzy number is reduced to a triangular fuzzy number denoted by $A=(a,b,d,\omega)$ or $A=(a,b,d)$ if $\omega=1$.Therefore, triangular fuzzy numbers are special cases of trapezoidal fuzzy numbers.
Since L_A and R_A are both strictly monotonical and continuous functions, their inverse functions exist and should be continuous and strictly monotonical. Let $L_A^{-1}:[a,b]\to[0,\omega]$ and $R_A^{-1}:[a,b]\to[0,\omega]$ be the inverse functions of $L_A(x)$ and $R_A(x)$, respectively. Then $L^{-1}{}_A(r)$ and $R^{-1}{}_A(r)$ should be integrable on the close interval $[0,\omega]$. In other words, both $\int_0^{\omega} L_A^{-1}(r)dr$ and

$\int_0^{\omega} R_A^{-1}(r)dr$ should exist. In the case of trapezoidal fuzzy number, the inverse functions $L^{-1}{}_A(r)$ and $R^{-1}{}_A(r)$ can be analytically expressed as

$$L_A^{-1}(r) = a + (b-a)r/\omega \qquad 0 \le \omega \le 1 \tag{2}$$

$$R_A^{-1}(r) = d - (d-c)r/\omega \qquad 0 \le \omega \le 1 \tag{3}$$

The set of all elements that have a nonzero degree of membership in A, it is called the support of A, i.e.

$$Supp(A) = \{x \in X \mid \mu_A(x) \succ 0\} \tag{4}$$

The set of elements having the largest degree of membership in A, it is called the core of A, i.e.

$$Core(A) = \left\{ x \in X \mid \mu_A(x) = \sup_{x \in X} L_A(A) \right\} \tag{5}$$

In the following, we will always assume that A is continuous and bounded support Supp (A). The strong support of A should be $Supp(A) = [a, d]$.

2.1 Definition

A function $s:[0,1] \to [0,1]$ is a reducing function if is s increasing and $s(0) = 0$ and $s(1) = 1$. We say that s is a regular function if $\int_0^1 s(r)dr = 1/2$.

2.2 Definition

If A is a fuzzy number with r-cut representation, $\left(L_A^{-1}(r), R_A^{-1}(r)\right)$ and s is a reducing function, then the value of A (with respect to s); it is defined by

$$Val(A) = \int_0^1 s(r)[L_A^{-1}(r) + R_A^{-1}(r)]dr \tag{6}$$

2.3 Definition

If A is a fuzzy number with r-cut representation $\left(L_A^{-1}(r), R_A^{-1}(r)\right)$, and s is a reducing function then the ambiguity of A (with respect to s) is defined by

$$Amb(A) = \int_0^1 s(r)[R_A^{-1}(r) - L_A^{-1}(r)]dr \tag{7}$$

2.4 Definition

The addition and scalar multiplication of fuzzy numbers are defined by the extension principle and can be equivalent represented in [30, 31, 32] as follows.

For arbitrary $A=\left(L_A^{-1}(r),R_A^{-1}(r)\right)$ and $B=\left(L_B^{-1}(r),R_B^{-1}(r)\right)$ we define addition $(A+B)$ and multiplication by scalar $k\succ 0$ as

$$\begin{aligned}&(\underline{A+B})(r)=\underline{A}(r)+\underline{B}(r)\\&(\overline{A+B}(r))=\overline{A}(r)+\overline{B}(r)\\&(\underline{kA})(r)=k\,\underline{A}(r),(\overline{kA})(r)=k\,\overline{A}(r).\end{aligned}\tag{8}$$

To emphasis the collection of all fuzzy numbers with addition and multiplication as defined by (8) is denoted by E, which is a convex cone. The image (opposite) of $A=(a,b,c,d)$ is $-A=(-d,-c,-b,-a)$ (see [32, 33]).

3. New similarity measure for triangular fuzzy numbers

Let $A=(a_1,a_2,a_3)$ and $B=(b_1,b_2,b_3)$ be two arbitrary triangular fuzzy numbers. We define the distance between A and B as

$$d(A,B)=\frac{a_1+2a_2+a_3}{4}-\frac{b_1+2b_2+b_3}{4}\tag{9}$$

Moreover, maximum and minimum of a triangular fuzzy number will be defined as

$$\max(A,B)=\left(\max\{a_1,b_1\},\max\{a_2,b_2\},\max\{a_3,b_3\}\right)$$
$$\min(A,B)=\left(\min\{a_1,b_1\},\min\{a_2,b_2\},\min\{a_3,b_3\}\right)$$

also we consider $x_A=\dfrac{a_1+a_2+a_3}{3}$ as the centroid point of fuzzy number M .

Now let $A_1,A_2,...,A_n$ are triangular fuzzy number. The new index for each fuzzy number is

$$Index(A_i)=\frac{d(A_i,A_{\min})}{d(A_{\max},A_i)}\times x_A\tag{10}$$

Consequently the ranking order will be according to the following relation

$Index_M\le Index_N$ if and only if $M\le N.$

3.1 Example

Consider three triangular fuzzy numbers $A=(5,6,7),B=(5.9,6,7)$ **and** $C=(6,6,7)$.

we can get that

$$A_{\max}=(\max\{5,5.9,6\},\max\{6,6,6\},\max\{7,7,7\})=(6,6,7)$$
$$A_{\min}=(\min\{5,5.9,6\},\min\{6,6,6\},\min\{7,7,7\})=(5,6,7)$$

$$d(TFN_{\max}, A) = \frac{6+2\times 6+7}{4} - \frac{5+2\times 6+7}{4} = 0.25$$
$$d(TFN_{\max}, B) = \frac{6+2\times 6+7}{4} - \frac{5.9+2\times 6+7}{4} = 0.025$$
$$d(TFN_{\max}, C) = \frac{6+2\times 6+7}{4} - \frac{6+2\times 6+7}{4} = 0$$

$$d(A, TFN_{\min}) = \frac{5+2\times 6+7}{4} - \frac{5+2\times 6+7}{4} = 0$$
$$d(B, TFN_{\min}) = \frac{5.9+2\times 6+7}{4} - \frac{5+2\times 6+7}{4} = 0.225$$
$$d(C, TFN_{\min}) = \frac{6+2\times 6+7}{4} - \frac{5+2\times 6+7}{4} = 0.25$$

$x_A = 6, x_B = 6.30$ and $x_C = 6.33$

Consequently, the new index for each fuzzy number will be computed in below

$$Index(A) = \frac{0}{0.25} \times 6 = 0$$
$$Index(B) = \frac{0.225}{0.025} \times 6.30 = 56.7$$
$$Index(A) = \frac{0.25}{0} \times 6.33 = \infty .$$

Hence the ranking order is $A \prec B \prec C$.

To compare the proposed method with some of previous method we refer the reader to Table 1.

Table. 1

Fuzzy number **Method**	**A**	**B**	**C**
Cheng,CV-index	0.028	0.0098	0.0089
Chu and Tsao	3	3.126	3.085
Yager	36.03	39.69	40.07
Lee and Li	6	6.30	6.33
Asady and Zendehnam	6	6.22	6.25
Chen and Hsieh	6	6.15	6.17

4. Conclusion

With the increasing development of fuzzy set theory in various scientific fields and the need to compare fuzzy numbers in different areas, the method can provide results currently ranking methods with ease and less time to the very useful and will be applied. In this research an index for ranking fuzzy numbers, which introduced the features and needs of researchers in this field will be useful.

Acknowledgment

This work was partly supported by Islamic Azad University, Firuz-Kuh Branch.

References

1. R. Jain. Decision-making in the presence of fuzzy variable. *IEEE Transactions on Systems, Man, and Cybernetics*, 6:698-703, 1976.
2. R. Jain. A procedure for multi-aspect decision making using fuzzy sets. *International Journal of Systems Science*, 8:1-7, 1977.
3. S. Bass and H. Kwakernaak. Rating and ranking of multiple-aspect alternatives using fuzzy sets. *Automatica*, 13:47-58, 1977.
4. D. Dubios and H. Prade. Operations on fuzzy numbers. *International Journal of Systems Science*, 9:613-626, 1978.
5. J.F. Baldwin and N.C.F. Guild. Comparison of fuzzy numbers on the same decision space. *Fuzzy Sets and Systems*, 2:213-233, 1979.M.
6. Adamo. Fuzzy decision trees. *Fuzzy Sets and Systems*, 4:207-219, 1980.

7. W.K. Chang. Ranking of fuzzy utilities with triangular membership functions. *International Conference on Plicy Analysis and Information Systems, Tamkang University*, 163-171, 1981.
8. R.R. Yager. On choosing between fuzzy subsets. *Kybernetes*, 9:151-154, 1980.
9. R.R. Yager. A procedure for ordering fuzzy subests of the unit interval. *Information Sciences*, 24:143-161,1981.
10. G. Bortolan and R. Degani. A review of some methods for ranking fuzzy numbers. *Fuzzy Sets and Systems*, 15:1-19, 1985.
11. S.J. Chen and C.L. Hwang. *Fuzzy multiple Attribute Decision Making*. Spinger-Verlag, Berlin, 1992.
12. S. Chen, Ranking fuzzy numbers with maximizing set and minimizing set. *Fuzzy Sets and Systems*, 17:113-129, 1985.
13. F. Choobineh and H. Li. An index for ordering fuzzy numbers. *Fuzzy Sets and Systems*, 54:287-294, 1993.
14. C.H. Cheng. A new approach for ranking fuzzy numbers by distance method. *Fuzzy Sets and Systems*, 95:307-317, 1998.
15. T. Chu and C. Tsao. Ranking fuzzy numbers with an area between the centroid point and original point. *Computers and Mathematics with Applications*, 43:111-117, 2002.M.
16. Ma and A. Kandel and M. Friedman. A new approach for defuzzification. *Fuzzy Sets and Systems*, 111:351-356, 2000.
17. S. Abbasbandy and B. Asady. A Note on “A new approach for defuzzification”. *Fuzzy Sets and Systems*, 128:131-132, 2002.
18. S. Abbasbandy and M. Amirfakhrian. A new approach to universal approximation of fuzzy functions on a discrete set of points. *Applied Mathematical Modeling*, 30:1525-1534, 2006.
19. S. Abbasbandy and M. Amirfakhrian. The nearest trapezoidal form of a generalized left right fuzzy number. *International Journal of Approximate Reasoning*, 43:166 178, 2006.
20. .S. Abbasbandy and B. Asady. Ranking of fuzzy numbers by sign distance. *Information Sciences*, 176:2405-2416, 2006.
21. L.H. Chen and H.W. Lu. An approximate approach for ranking fuzzy numbers based on left and right dominance. *Computers and Mathematics with Applications*, 41:1589-1602, 2001.
22. T. Hajjari, Ranking of Fuzzy Numbers Based on Ambiguity Degree, Australian Journal of Basic and Applied Sciences, 5(1) 62-69, 2011.
23. T. Hajjari, Ranking of Fuzzy Numbers by Middle of Expected Interval, In: First International Conference in Mathematics and Statistics, Sharjah, 2010.
24. S. Abbasbandy and T. Hajjari. A new approach for ranking of trapezoidal fuzzy numbers. *Computers and Mathematics with Applications*, 57:413-419, 2009.
25. T. Hajjari, Comparison of Fuzzy numbers by Modified Centroid Point Method. In: Third International Conference in Mathematical Sciences Dubai, 2008 , pp. 1139-1145.
26. T. Hajjari, Fuzzy Euclidean Distance for Fuzzy Data, In: 8th Iranian Conference on Fuzzy Systems, Iran , 2008, pp. 127-132.
27. T. Hajjari, Ranking Fuzzy Numbers by Sign Length, In: 7th Iranian Conference on Fuzzy Systems, Iran 2007, pp. 297-301.
28. B. Asady and A. Zendehnam, Ranking fuzzy numbers by distance minimization, Appl. Math. Model. 31 (2007) 2589-2598.

29. B. Asady, Revision of distance minimization method for ranking fuzzy numbers, Appl. Math. Model. 35 (2011) 1306-1311.
30. R. Goetschel and W. Voxman. Elementary calculus. *Fuzzy Sets and Systems*, 18:31-43, 1986.
31. M. Ma and M. Friedman and A. Kandel. A new fuzzy arithmetic. *Fuzzy Sets and Systems*, 108:83-90, 1999.
32. D. Dubois and H. Prade. *Fuzzy Sets and System: Theory and Application*. Academic Press, New York, 1980.
33. L.A. Zadeh. Fuzzy sets. *Information and Control*, 8:338-353, 1965.

Proceedings, 4th Chaotic Modeling and Simulation International Conference
31 May – 3 June 2011, Agios Nikolaos, Crete Greece

Search for Deterministic Nonlinearity in the Light Curves of the Black Hole System GRS 1915+105

K. P. Harikrishnan[1], R. Misra[2], and G. Ambika

[1] Department of Physics, The Cochin College, Cochin - 682 002, India
(E-mail: *kp_hk2002@yahoo.co.in*)
[2] Inter University Centre for Astronomy and Astrophysics, Pune - 411 007
(E-mail: rmisra@iucaa.ernet.in)
[3] Indian Institute of Science Education and Research, Pune - 411 021, India
(E-mail: g.ambika@iiserpune.ac.in)

Abstract. GRS 1915+105 is prominent black hole system exhibiting variability over a wide range of time scales and the light curves from the source have been classified into 12 temporal states. Here we undertake an analysis of the light curves from all the states using three important quantifiers from nonlinear time series analysis, namely, the correlation dimension (D_2), the correlation entropy (K_2) and singular value decomposition (SVD). An important aspect of our analysis is that, for estimating these quantifiers, we use algorithmic schemes which we have proposed recently and tested successfully on synthetic as well as practical time series from various fields. We show that nearly half of the 12 temporal states exhibit deviation from randomness and their complex temporal behavior can be approximated by a few (3 or 4) coupled ordinary differential equations. Based on our results, the 12 states can be broadly classified into three from a dynamical perspective: purely stochastic with D2 tending to infinity, affected by colored noise and those which are potential candidates for deterministic non linearity with $D2 \leq 4$. Our results could be important for a better understanding of the processes that generate the light curves and hence for modeling the temporal behavior of such complex systems.
Keywords: Time Series Analysis, Applied Chaos, Black Hole Binaries.

1 Introduction

Most of the systems in Nature are described by models which are inherently nonlinear. Since the discovery of *deterministic chaos* a few decades back and the development of various techniques in subsequent years, there remained the exciting prospect of a better understanding of the complex behavior shown by various natural systems in terms of simple nonlinear models. A large number of techniques from nonlinear dynamics are routinely being employed for this purpose. For example, see Hilborn [1] and Lakshmanan & Rajasekhar [2] for details.

Astrophysical objects are among the most interesting real world syatems where methods from nonlinear dynamics have been attempted right from the development of chaos theory. Important examples include the analysis of variable stars [3] to understand the nature of variability, the study of the temporal variations in the sun spot activities [4] and to develop possible measures to differentiate between AGNs and black holes [5]. One major limitation regarding the analysis of astrophysical objects is that the only available information regarding the source is the light intensity variations emitted by it, called the *light curve*, over which one has no control. It is a single scalar variable recorded as a function of time, namely, a *time series*. Thus the main task in the analysis is to understand the nature of variability and to reconstruct the underlying model using the methods of time series analysis.

A number of computational schemes and measures are used for the nonlinear time series analysis as discussed by many authors [6,7]. The most important quantifiers among these are the correlation dimension (D_2) and the correlation entropy (K_2). We have recently proposed automated algorithmic schemes [8,9] for computation of D_2 and K_2 from time series based on the delay embedding technique and applied them successfully to various types of time series data. In this work, we apply these computational schemes to analyse the X-ray light curves from a very prominent black hole binary, GRS 1915+105.

2 Analysis of the Light Curves

Among the most important nonlinearity measures used for the analysis of time series data are D_2 and K_2. D_2 is often used as a discriminating measure for hypothesis testing to detect nontrivial structures in the time series. However, if the time series involves colored noise, a better discriminating measure is considered to be K_2 [10]. We employ surrogate analysis using both D_2 and K_2 as discriminating measures and to compute these measures, we make use of the automated algorithmic schemes proposed by us recently [8,9]. The scheme involves creation of an embedding space of dimension M with delay vectors x_j constructed from the time series. One then counts the relative number of data points in the embedded attractor within a distance R from a particular i^{th} data point

$$p_i(R) = \lim_{N_v \to \infty} \frac{1}{N_v} \sum_{j=1, j \neq i}^{N_v} H(R - |\boldsymbol{x_i} - \boldsymbol{x_j}|) \tag{1}$$

where N_v is the total number of reconstructed vectors and H is the Heaviside step function. Averaging this quantity over N_c number of randomly selected centres gives the correlation sum

$$C_M(R) = \frac{1}{N_c} \sum_{i}^{N_c} p_i(R) \tag{2}$$

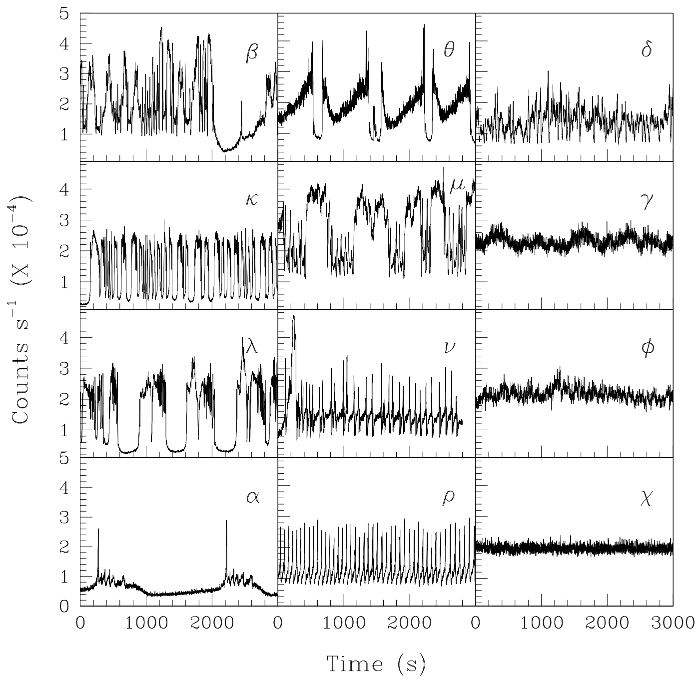

Fig. 1. Light curves from the 12 temporal states of the black hole system GRS 1915+105. Only a part of the generated light curve is shown for clarity.

The correlation dimension $D_2(M)$ is then defined to be,

$$D_2 \equiv \lim_{R \to 0} d(logC_M(R))/d(log(R)) \tag{3}$$

which is the scaling index of the variation of $C_M(R)$ with R as $R \to 0$. In our scheme, D_2 is computed by choosing a scaling region algorithmically.

To compute K_2, one measures the ratio at which the trajectory segments are increased as M increases, using the formal expression

$$K_2 \Delta t \equiv \lim_{R \to 0} \lim_{M \to \infty} \lim_{N \to \infty} log(C_M(R)/C_{M+1}(R)) \tag{4}$$

To generate the surrogate data sets, we apply the IAAFT scheme [11,12] using the TISEAN package [7]. Finally, in order to visualise the qualitative features of the underlying attractor, we use the singular value decomposition (SVD) analysis (for details, see [9]). The SVD analysis computes the dominant eigen vectors whose projection, called the BK projection, shows the reconstructed attractors from the time series. Here we use the TISEAN package to generate the SVD plots.

The black hole source under investigation in this work, GRS 1915+105, is unique among all such sources in that it shows a wide range of variability

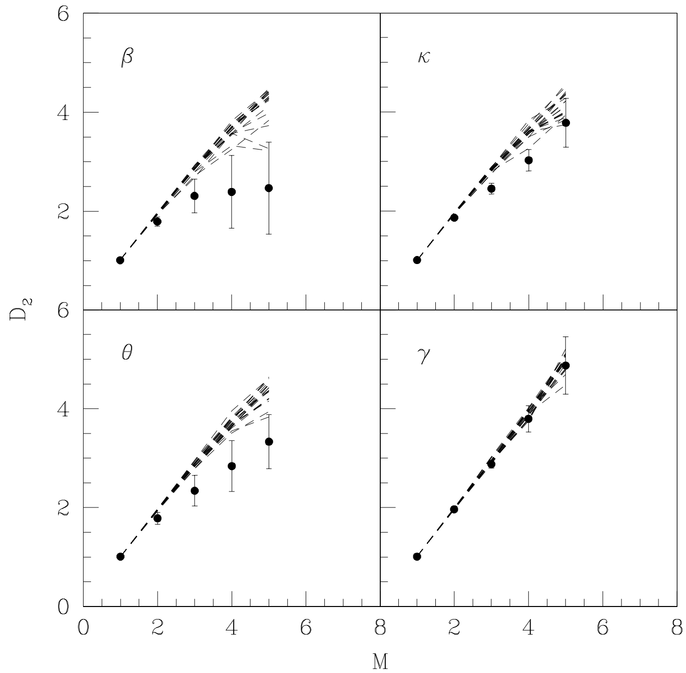

Fig. 2. Surrogate analysis with D_2 as a discriminating measure for the light curves from four states of GRS 1915+105. Surrogates are represented by dashed lines without error bar. Note that the null hypothesis can be rejected in all cases except the γ state.

in the light curves. Belloni et al. [13] have classified the light curves into 12 spectroscopic classes based on the RXTE observations. The nature of the light curves changes completely as the system flips from one temporal state to another. We have chosen a representative data set from each temporal class and extracted continuous data streams 3200 seconds long from it. The light curves were generated with a time resolution of 0.5 seconds resulting in approximately 7000 continuous data points for each class. More details regarding the data are given elsewhere [14].

Fig.1 shows all the 12 light curves used for the analysis, which are labelled by 12 different symbols representing the 12 temporal states of the black hole system. An earlier analysis of these light curves has shown that more than half of these 12 states deviated from a purely stochastic behavior [15]. Here we combine the results of D_2, K_2 and SVD analysis to get a better understanding regarding the nature of these light curves.

Fig.2 and Fig.3 show the results of surrogate analysis on eight different states. It is clear that, of the states shown in the the two figures, only two - γ and ϕ - show purely stochastic behavior. Of the remaining four states, two

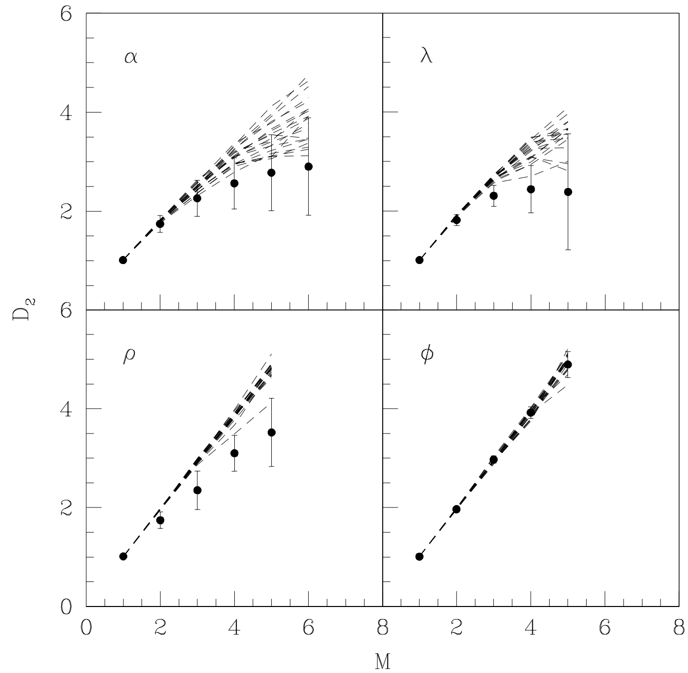

Fig. 3. Same as the previous figure, with four other states. Again, only one state, ϕ, is consistent with noise.

more, namely δ and χ, are found to belong to this category. Thus, only four out of the 12 states show behavior consistent with white noise in D_2 analysis.

It is known that the X-ray emissions from the accretion discs may also involve colored noise. The colored noise gives a saturated value of D_2 and hence it is difficult to identify it in D_2 analysis. For this, we undertake surrogate analysis with K_2 as discriminating statistic. While data involving nontrivial structures give a saturated value of K_2, for pure colored noise, $K_2 \rightarrow 0$ as the embedding dimension M is increased. Results of K_2 analysis for four representative states are shown in Fig.4. While the behavior of β, θ and γ are consistent with earlier D_2 analysis, the bahavior of κ suggests that it is contaminated with colored noise. In fact 3 of the 8 states - κ, λ and μ - which showed deviation from stochastic behavior in the D_2 analysis are found to be contaminated with colored noise in the K_2 analysis.

Finally, we perform a SVD analysis on all the states which clearly shows the qualitative nature of the underlying attractors. The plot of attractors for selected states is shown in Fig.5. The most interesting plot is for the ρ state which shows a typical limit cycle type attractor added with noise. Also, note that the SVD plot for the κ state has nontrivial appearance, eventhough the

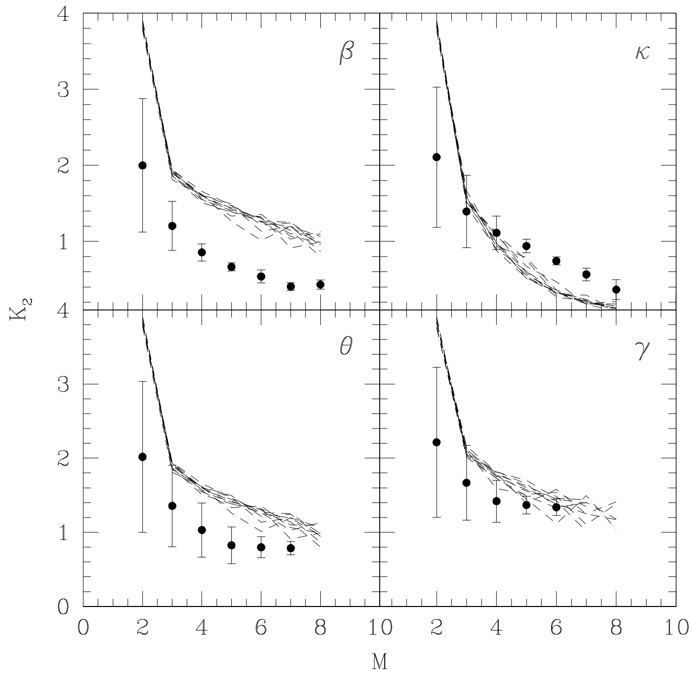

Fig. 4. Surrogate analysis of the light curves from four states with K_2 as the discriminating measure. While the data and the surrogates can be distinguished for β and θ, κ and γ behaves like colored noise and white noise respectively.

surrogate analysis suggested the presence of colored noise. This may be an indication that the state is not a pure colored noise. The same behavior is found for two other states, λ and μ. Thus, these 3 states are likely to be a mixture of deterministic nonlinearity and colored noise.

Based on our results, the 12 states can thus be divided into 3 broader classes from the point of view of their temporal properties. It turns out that some of the states which are spectroscopically different, behave identically in their nonlinear dynamics characteristics. This may be an indication of of some common features in the mechanism of production of light curves from these states.

3 Conclusion

Identifying nontrivial structures in real world systems is considered to be a challenging task as it requires a succession of tests using various quantitative measures. Eventhough a large number of potential systems from various fields have been analysed so far, the results remain inconclusive in most

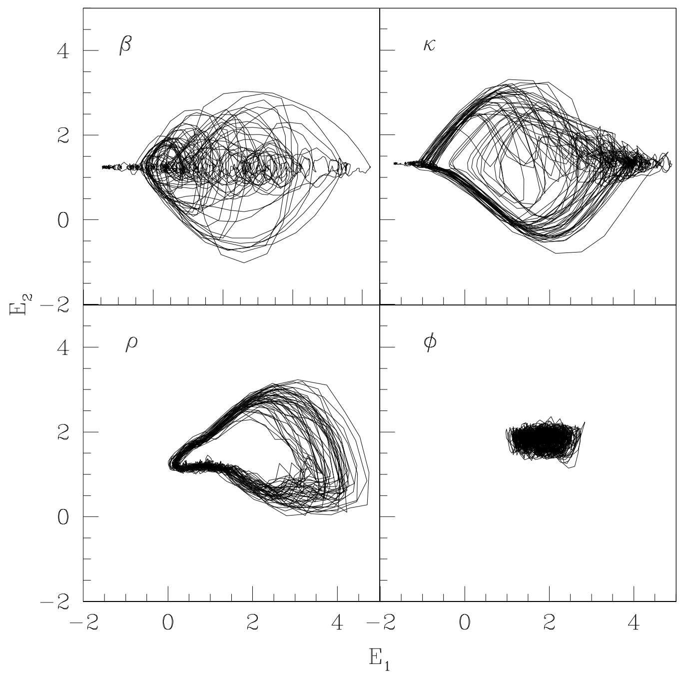

Fig. 5. The plot of attractors underlying four states of the black hole system reconstructed via SVD analysis. Except the ϕ state, which behaves as a white noise, all the others indicate the presence of underlying attractors, the most interesting being the ρ state.

cases. Here we present an interesting example of an astrophysical system, which we analyse using several important quantifiers of nonlinear dynamics. We find that out of the 12 spectroscopic states of the black hole system, only 4 are purely stochastic. The remaining states show signatures of deterministic nonlinearity, with 3 of them contaminated by colored noise. All these 8 states are found to have $D_2 < 4$ so that their complex temporal behavior can be approximated by 3 or 4 coupled ordinary differential equations. Based on our results, the 12 states can be broadly classified into 3 from a dynamical perspective: purely stochastic with $D_2 \to \infty$, affected by colored noise and those which show deterministic nonlinear behavior with $D_2 < 4$.

KPH and RM acknowledge the financial support from Department of Science and Technology, Govt. of India, through a research grant No. SR/SP/HEP-11/2008.

References

1.R. C. Hilborn. *Chaos and Nonlinear Dynamics*, New York, 1994, Oxford University Press.
2.M. Lakshmanan and S. Rajasekhar. *Nonlinear Dynamics*, New York, 2003, Springer.
3.J. R. Buchler and Z. Kollath. Strange Cepheids and RR Lyrae. *Astrophys. J.*, 555:961, 2001.
4.N. Jevtic, J. S. Schweitzer and C. J. Cellucci. Nonlinear time series analysis of northern southern hemisphere daily sunsspot numbers in search of short term chaotic behavior. *Astronomy and Astrophys.*, 379:611, 2001.
5.M. Gliozzi, C. Rath, I. E. Papadakis and P. Reig. Characterising black hole variability with nonlinear methods: the case of X-ray Nova 4U 1543-47. *Astronomy and Astrophys.*, 512:21, 2010.
6.H. Kantz and T. Screiber. *Nonlinear Time Series Analysis*, Cambridge, 1997, Cambridge University Press.
7.R. Hegger, H. Kantz and T. Schreiber. Practical implementation of nonlinear time series methods: The TISEAN package. *Chaos*, 9:413, 1999.
8.K. P. Harikrishnan, R. Misra, G. Ambika and A. K. Kembhavi. A non subjective approach to the GP algorithm for analysing noisy time series. *Physica D*, 215:137, 2006.
9.K. P. Harikrishnan, R. Misra and G. Ambika. Combined use of correlation dimension and entropy as discriminating measures for time series analysis. *Comm. Nonlinear Sci. Num. Simulations*, 14:3608, 2009.
10.M. B. Kennel and R. Isabelle. A method to distinguish possible chaos from colored noise and to determine embedding parameters. *Phys. Rev. A*, 46:3111, 1992.
11.T. Schreiber and A Schmitz. Improved surrogate data for nonlinearity tests. *Phys. Rev. Lett.*, 77:635, 1996.
12.T. Schreiber and A. Schmitz. Surrogate time series. *Physica D*, 142:346, 2000.
13.T. Belloni, M. Klein-Wolt, M. Mendez, M. van der Klis and van Paradjis. A model independent analysis of the variability of GRS 1915+105. *Astronomy and Astrophys.*, 355:271, 2000.
14.R. Misra, K. P. Harikrishnan, B. Mukhopadhyay, G. Ambika and A. K. Kembhavi. The chaotic behavior of the black hole system GRS 1915+105. *Astrophys. J*, 609:313, 2004.
15.R. Misra, K. P. Harikrishnan, G. Ambika and A. K. Kembhavi. The nonlinear behavior of the black hole system GRS 1915+105. *Astrophys. J*, 643:1114, 2006.